Research Paper

Marine Biomass-Assisted Fabrication of Iron Oxide Nanoparticles for Methyl Red Adsorption, Larvicidal Activity and Hemolysis Assessment

A. Malarvizhi[1], C. Stella Packiam[1*], M. I. Delighta Mano Joyce[2], A. Dhivya[3]

[1]Research Scholar (22212012032001), Department of Chemistry, A.P.C. Mahalaxmi College for Women affiliated with Manonmaniam Sundaranar University, Tirunelveli-627012, (Tamil Nadu), India

[1*]Research Guide, Department of Chemistry, A.P.C. Mahalaxmi College for Women, Tuticorin-628002, (Tamil Nadu), India

[2]Department of Chemistry, St. Joseph's College of Engineering, Chennai-600119, Tamil Nadu, India

[3]Department of Zoology, Sadakathullah Appa College, Tirunelveli, Tamil Nadu, India

***Corresponding Author: C. Stella Packiam | Email: stellapackiam@apcmcollege.ac.in**

ABSTRACT

This study reports an eco-friendly approach for synthesizing iron oxide nanoparticles using marine squid (Sepioteuthis lessoniana) biomass as a natural reducing and stabilizing agent. The biosynthesized nanoparticles (Sl-FeONAs) were evaluated for adsorptive removal of methyl red (MR) dye, larvicidal activity and hemolytic safety. Structural and morphological characteristics of Sl-FeONAs were confirmed by UV–visible spectroscopy, FTIR, XRD, SEM and EDX analyses, indicating the successful formation of nanoscale iron oxide particles capped with biomolecules. Adsorption experiments demonstrated rapid dye removal, with maximum efficiency of approximately 88% under optimal conditions (pH 6, 60 min contact time and suitable adsorbent dosage). The adsorption behavior was better described by the Freundlich isotherm model, suggesting heterogeneous surface adsorption and multilayer formation. In addition, the synthesized nanoparticles exhibited significant larvicidal activity against mosquito larvae while showing minimal hemolytic effects at lower concentrations, indicating good biocompatibility. These findings highlight the potential of marine biomass-mediated iron oxide nanoparticles as sustainable multifunctional materials for wastewater treatment and vector control applications.

Keywords: Sepioteuthis lessoniana, larvicidal activity, Freundlich isotherm model, Adsorption experiments, Hemolytic effects.

How to cite this article: Malarvizhi A, Stella Packiam C, Delighta Mano Joyce MI, Dhivya A. Marine Biomass-Assisted Fabrication of Iron Oxide Nanoparticles for Methyl Red Adsorption, Larvicidal Activity and Hemolysis Assessment. Int J Drug Deliv Technol. 2026;16(55s): 876-895. DOI: 10.25258/ijddt.16.55s.88

Source of support: Nil.

Conflict of interest: None.

INTRODUCTION

Marine organisms represent an abundant and largely unexplored source of bioactive compounds with unique biochemical compositions. In particular, marine molluscs such as **squid (*Sepioteuthis lessoniana*)** contain various proteins, polysaccharides and secondary metabolites that can facilitate the green synthesis of iron oxide nanoparticles. The utilization of marine biomass for nanoparticle synthesis offers advantages such as sustainability, cost-effectiveness and enhanced functional performance due to the presence of natural capping agents. Furthermore, marine biomass-derived nanoparticles may exhibit improved biological activities, making them suitable for environmental and biomedical applications [7,8].

Conventional methods for synthesizing iron oxide nanoparticles often involve chemical reagents and high energy consumption, which may generate toxic by-products and pose environmental risks. To overcome these limitations, **green synthesis approaches** using biological resources have gained increasing attention. Biological materials such as plant extracts, microorganisms and marine

organisms contain diverse biomolecules that can act as natural reducing and stabilizing agents in nanoparticle synthesis. These eco-friendly approaches not only minimize the use of hazardous chemicals but also improve the biocompatibility and functional properties of the synthesized Nanoparticles [5,6].

Adsorption is considered one of the most effective, eco-friendly and cost-effective techniques for removing organic pollutants like **methyl red (MR)** widely used in textile, pharmaceutical and chemical industries from aqueous systems due to its operational simplicity, high efficiency and low energy requirement [1,2].

In recent years, nanomaterials have attracted considerable attention as promising adsorbents because of their high surface area, abundant active sites and enhanced reactivity. Among various nanomaterials, **iron oxide nanoparticles (IONPs)** have emerged as attractive candidates for environmental remediation owing to their magnetic properties, chemical stability and strong adsorption capability toward various organic contaminants. These nanoparticles can effectively interact with dye molecules through electrostatic interactions, surface complexation and other physicochemical mechanisms, facilitating efficient pollutant removal from wastewater [3,4].

In addition to wastewater treatment, nanomaterials have also been explored for **vector control and biomedical applications**. Mosquito-borne diseases such as dengue, malaria and chikungunya continue to pose significant public health challenges worldwide. IONPs synthesized through biological routes have demonstrated promising **larvicidal activity** against mosquito larvae by disrupting cellular and physiological processes [9].

Inorder to assess larvicides in vector control p rograms and make sure that the products are s afe for use in the environment, this paper is crucial [5]. Evaluating the **hemolytic activity** of IONPs is essential for determining their blood compatibility and potential biomedical safety. Materials exhibiting less than 5 % hemolysis are generally considered biocompatible and suitable for biological applications [10,11].

The present study focuses on the **green synthesis of IONPs** and the evaluation of their multifunctional applications. The findings of this study aim to provide insights into the development of sustainable marine biomass-derived IONPs **using marine squid (*Sepioteuthis lessoniana*) extract** for environmental remediation and potential biomedical applications. The synthesized IONPs nanoparticles were characterized and investigated for their **adsorptive removal of methyl red dye from aqueous solutions**, **larvicidal efficacy against mosquito larvae** and **hemolytic activity to assess biocompatibility** aiming to develop a sustainable and multifunctional material for environmental remediation.

EXPERIMENTAL

Ferric chloride ($FeCl_3$) used in this study was procured from the laboratory of A.P.C. Mahalaxmi College, Thoothukudi and all solutions were prepared using triple-distilled deionized water. Fresh marine squid samples were collected from the commercial fish market at Threspuram, Thoothukudi, on 23rd January 2023 and the selected species was processed for further analysis. The collected samples were thoroughly washed, oven-dried and preserved in airtight containers until use.

Fig. -1: ***Sepioteuthis lessoniana***

Spectrophotometric analyses were performed using an Elico SC-177 scanning mini spectrophotometer to record absorbance at different concentrations of the ethanolic extract. Biochemical constituents were quantified following standard protocols: total carbohydrates were estimated by the Anthrone method [12,13], total proteins were determined using the method described by Lowry et al. [14,15], total lipids were analyzed according to the procedure of Bragdon [16] and total phenolic and flavonoid contents were evaluated using the Folin–Ciocalteu reagent method [17,18]. Furthermore, the chemical composition of the extract was analyzed by gas chromatography–mass spectrometry (GC–MS) using a PerkinElmer GC Clarus 500 system equipped with an AOC-20i autosampler, where the gas chromatograph was interfaced with a mass spectrometer, following established analytical conditions. Synthesised FeO-NPs were analyzed using UV-Vis JASCO V-600 spectrophotometer. The functional groups of marine squid ethanol extract was detected with Fourier transform infrared spectrometer (FT-IR) using SHIMADUZU (Miracle 10). The Scanning Electron Microscope (SEM) with EDAX attachment (CF) was used for the morphology, size and percentage of element composition by TESCAN MIRA3 XMU. X'Pert Pro PANalytical was used for observing the crystal shape of IONPs.

Marine Biomass Extraction from *Sepioteuthis lessoniana*

The collected marine mollusc specimens were initially rinsed thoroughly with seawater to remove loosely attached debris. Subsequently, epibionts and adhering materials such as sand particles and shell fragments were carefully removed manually. The cleaned samples were transported to the laboratory and washed again with distilled water to eliminate residual impurities. The specimens were then shade-dried at room temperature and homogenized to obtain a coarse powdered material, following standard marine biomass preparation protocols [19,20]. For biomolecule extraction, 0.5 g of the dried powdered sample was finely ground using a sterile mortar and pestle with a tenfold volume of 80 % ethanol. The homogenized mixture was centrifuged at 10,000 rpm for 20 min and the resulting supernatant containing soluble biomolecules was collected. The residual biomass was further re-extracted with five times the volume of 80 % ethanol

to ensure maximum recovery of bioactive compounds. The mixture was again centrifuged under identical conditions and the supernatants obtained from both extraction steps were pooled and concentrated to dryness, following previously reported biomolecule extraction procedures [21,22].

Fabrication of Sl-FeONAs

For nanoparticle synthesis, 80 mL of 1 M aqueous ferric chloride solution was added dropwise to 20 mL of the marine mollusc extract under continuous stirring. The reaction mixture was centrifuged at 10,000 rpm for 30 min, and the resulting precipitate was washed repeatedly (2–3 times) with Millipore water to remove unreacted ions and impurities [23]. The final product was dried using a vacuum hot-air oven at 125 °C under 15 psi pressure for 120 min. The use of a vacuum environment minimizes oxidative interference and prevents contamination from atmospheric gases, ensuring the formation of phase-pure iron oxide nanoparticles Sl-FeONAs [24]

.

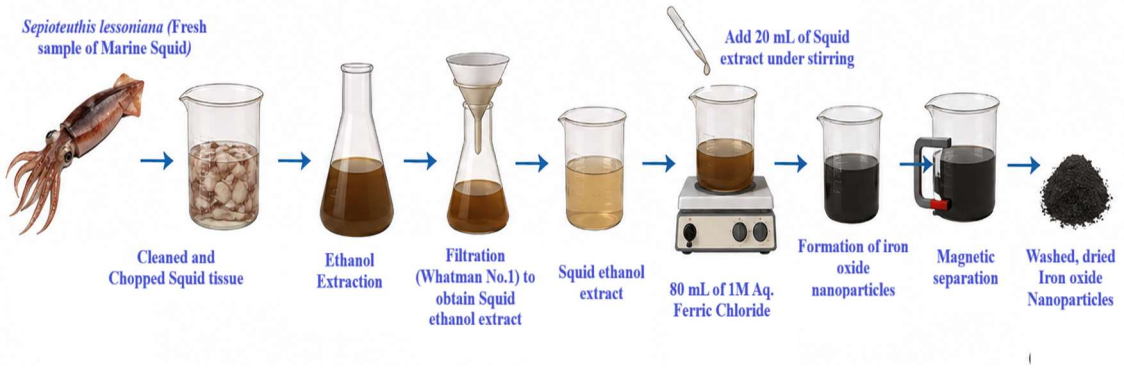

Fig. -2: Fabrication of Iron oxide NPs from *Sepioteuthis lessoniana*

Adsorption Test Using Methyl Red Dye

A stock solution of methyl red (250 mg L^{-1}) was prepared and subsequently diluted to the desired concentrations for batch experiments. Predetermined amounts of iron oxide nanoparticles were dispersed in dye solutions of varying concentrations (40-250 mg L^{-1}). The suspensions were continuously stirred until equilibrium was attained. To maintain a constant ionic strength, NaCl was added to achieve a background electrolyte concentration of 0.01 M. Additional experiments were conducted at ionic strengths of 0.01 and 0.1 M to evaluate the influence of ionic strength on adsorption performance. After equilibrium, the suspensions were centrifuged, and the residual dye concentration in the supernatant was analyzed using UV–visible spectroscopy. All experiments were conducted in triplicate, and average values were reported.

Isotherm-Based Evaluation of Adsorption Performance

The adsorption performance of iron oxide nanoparticles (IONPs) toward methyl red (MR) dye was evaluated through batch adsorption experiments and equilibrium isotherm analysis. Adsorption isotherms describe the relationship between the quantity of adsorbate adsorbed per unit mass of adsorbent and the equilibrium concentration of the adsorbate in solution at constant temperature.

Batch adsorption experiments were carried out using an optimized adsorbent dosage of **0.1 g L^{-1}** at an initial solution **pH of 6**. The initial concentration of MR dye was

varied between **10 and 40 mg L⁻¹** to investigate the adsorption capacity of the synthesized nanoparticles. The adsorption suspensions were agitated at **100 rpm for 3 h** to ensure equilibrium conditions. However, equilibrium adsorption was experimentally attained within **15 min**, indicating the rapid adsorption kinetics of the synthesized nanoparticles.

The effect of solution pH on the removal efficiency of MR dye was also examined over a pH range of **2–10 (2, 4, 6, 8, and 10)**. After completion of the adsorption process, the residual dye concentration in the supernatant was determined using a UV–Vis spectrophotometer. The **removal efficiency (R%)** and **equilibrium adsorption capacity (q_e)** were calculated using the following equations:

$$R(\%) = \frac{C_0 - C_t}{C_0} \times 100$$

$$q_e = \frac{V(C_0 - C_e)}{m}$$

where C_0, C_t, and C_e (mg L^{-1}) represent the initial dye concentration, dye concentration at time *t*, and equilibrium dye concentration, respectively. **V (L)** denotes the volume of the dye solution and **m (g)** represents the mass of the adsorbent.

To understand the adsorption mechanism and surface interaction between MR dye molecules and IONPs, the equilibrium adsorption data were analyzed using several adsorption isotherm models, including **Langmuir, Freundlich isotherms**.

The **Langmuir isotherm model** was applied to evaluate monolayer adsorption onto a homogeneous surface containing a finite number of identical adsorption sites. The adsorption process can be represented as:

$$\square_{(\square\square)} + \square \rightleftharpoons \square\square$$

where **A** represents dye molecules in solution, **S** denotes vacant adsorption sites, and **AS** represents the adsorbed dye molecules. The Langmuir equation is expressed as:

$$\square_{\square} = \frac{\square_{\square\square\square}\square_{\square}\square_{\square}}{1 + \square_{\square}\square_{\square}}$$

where **qmax (mg g^{-1})** is the maximum monolayer adsorption capacity and **K_L (L mg^{-1})** is the Langmuir adsorption constant related to the affinity of adsorption sites. The linearized form of the Langmuir equation is:

$$\frac{\square_{\square}}{\square_{\square}} = \frac{1}{\square_{\square\square\square}\square_{\square}} + \frac{\square_{\square}}{\square_{\square\square\square}}$$

The **Freundlich isotherm model** was used to describe adsorption on heterogeneous surfaces and multilayer adsorption processes. The Freundlich equation is expressed as:

$$\square_{\square} = \square_{\square}\square_{\square}^{1/\square}$$

where **q_e (mg g^{-1})** is the amount of dye adsorbed at equilibrium, **C_e (mg L^{-1})** is the equilibrium dye concentration, and **K_F** and **n** are the Freundlich constants representing adsorption capacity and adsorption intensity, respectively. The linearized form of the Freundlich equation is given by:

$$\square\square\square\ \square_{\square} = \square\square\square\ \square_{\square} + \frac{1}{\square}\square\square\square\ \square_{\square}$$

The Temkin isotherm requires a uniform distribution of binding energies and a linear decre ase in sorption heat. According to this model, the heat of adsorption of all molecules in the layer would drop linearly with coverage due to indirect adsorbate/adsorbent interactions.[44,45]The Temkin isotherm has typically been applied in the following ways:

$$\mathbf{Q_e = RT\ b\ T\ ln\ K\ T + RT\ b\ T\ ln\ C_e}$$

The Temkin model constants KT and B=RT/b, which offer information about the heat of ad sorption (J/mol), can be derived by linearly graphing q_e vs $\ln C_e$ [39,40].

Isotherm modeling provides important information regarding adsorption capacity, surface properties, and the mechanism of interaction between dye molecules and the nanoparticle surface. Comparative analysis of different isotherm models enables identification of the most appropriate adsorption model and supports the design and optimization of nanoparticle-based adsorption systems for wastewater treatment applications.

Larvicidal Activity

The larvicidal activity of the synthesized iron oxide nanoparticles (FeO NPs) was evaluated against mosquito larvae using a standard bioassay procedure. Larvicidal assays are widely used to determine the efficacy of nanomaterials and bioactive compounds in controlling mosquito vectors responsible for transmitting various diseases such as malaria, dengue, and chikungunya. Mosquito larvae at the third or fourth instar stage were selected for the experiment because they are more sensitive and suitable for evaluating larvicidal potential.

For the bioassay, different concentrations of FeO NPs were prepared by dispersing the nanoparticle powder in distilled water with continuous stirring and mild sonication to obtain a uniform suspension. Groups of 20 healthy larvae were introduced into beakers containing 100 mL of test solutions with varying nanoparticle concentrations (e.g., 10, 20, 30, 40, and 50 µg mL^{-1}). A control group containing only distilled water without nanoparticles was maintained under identical experimental conditions. All experiments were performed in triplicate at room temperature[29,30].

The mortality of larvae was recorded after 24 h of exposure. Larvae were considered dead when they did not show any movement upon gentle probing with a glass rod. The percentage mortality was calculated using the following equation:

$$\square\square\square\square\square\square\ \square\square\square\square\square\square\square\square\square\ (\%) = \frac{\square\square\square\square\square\square\ \square\square\ \square\square\square\square\ \square\square\square\square\square\square}{\square\square\square\square\square\ \square\square\square\square\square\square\ \square\square\ \square\square\square\square\square\square} \times 100$$

When control mortality ranged between 5–20%, the observed mortality was corrected using Abbott's formula to obtain accurate results:

$$\square\square\square\square\square\square\square\square\square\ \square\square\square\square\square\square\square\square\square\ (\%) = \frac{(\square\square\square\square\square\square\square\ \square\square\square\square\square\square\square\square\square)}{(\square\square\square\square\square\square\square\ \square\square\square\square\square\square\square\square\square)} \times 100$$

The lethal concentrations required to kill 50% (LC_{50}) and 90% (LC_{90}) of larvae were determined using probit analysis. The larvicidal activity of FeO NPs may be attributed to their ability to penetrate the larval cuticle, generate oxidative stress, and disrupt cellular and physiological functions, ultimately leading to larval death. Nanoparticles can also damage the midgut epithelial cells and interfere with respiratory and enzymatic processes in mosquito larvae.

The results indicated that larval mortality increased with increasing nanoparticle concentration, demonstrating a clear dose-dependent larvicidal effect. Such findings suggest

that FeO NPs synthesized through biological routes could serve as effective and environmentally friendly agents for mosquito vector control[31,32].

Hemolysis assay

To determine the hemocompatibility of the prepared NPs, 2 ml of healthy RBCs were isolated from human blood and added to 4ml Dulbecco's phosphate-buffered saline (D-PBS) and then centrifugated at 10000 g for 5 min to isolate red blood cells (RBCs). The RBCs were further washed five times with 10 ml of D-PBS and finally diluted to 20 ml with D-PBS. 0.2 ml of diluted RBC suspension was exposed to 0.8 ml of the nanoparticle D-PBS suspension at a concentration of 5, 10, 25, 50, 100 µg/ml to make the final nanoparticle concentration 5, 10, 25, 50, 100 µg/ml (test group), distilled water (positive group), and D-PBS (negative group).

Every group was represented for four tubes. After incubation at room temperature for 4 h and centrifugation for 5 min at 10016g, 100 µl of the supernatant of all samples was transferred to a 96-well plate and the absorbance was measured by a microplate reader (TECAN Znfinite M200, Austria) at 577 nm with the 655 nm as a reference. The haemolytic degree was expressed by the hemolysis percent as the following formula:

$$\% \text{ Hemolysis} = \frac{(\square\square\square.\square\square\ \square\square\square\square\square\square - \square\square\square.\square\square\ \square\square\square\square\square\square\square\ \square\square\square\square\square\square\square)}{(\square\square\square.\square\square\ \square\square\square\square\square\square\square\ \square\square\square\square\square\square\square - \square\square\square.\square\square\ \square\square\square\square\square\square\square\ \square\square\square\square\square\square\square)} x100$$

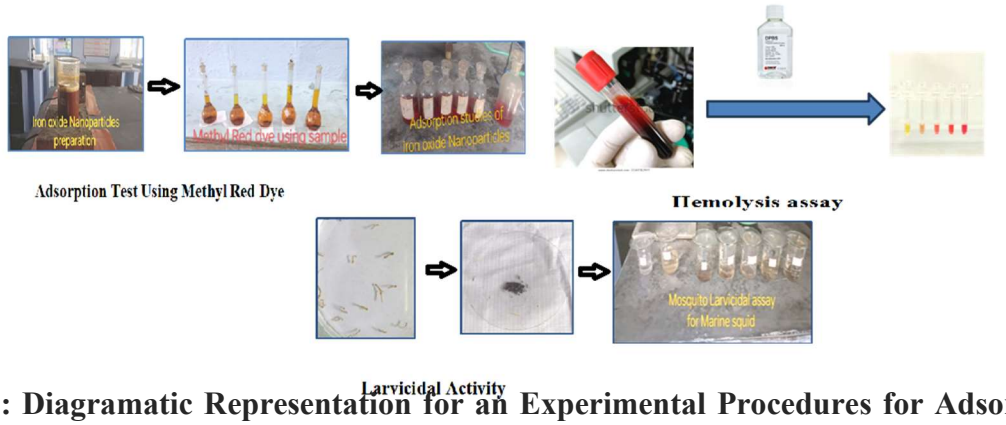

Fig. -3: Diagramatic Representation for an Experimental Procedures for Adsorption Studies, Larvicidal activity and Hemolysis assay for FeO Nanoparticle using Marine Squid *Sepioteuthis lessoniana*

RESULTS AND DISCUSSION

Spectrophotometric and Gas Chromatography-Mass Spectrometry (GC-MS) analysis:

Spectrophotometric analysis of squid extracts showed varying efficiencies in extracting carbohydrates, proteins, lipids, flavonoids, and phenols. Ethanol demonstrated the highest extraction capability, yielding significantly elevated levels of most biomolecules, with carbohydrates (40 %), proteins (14.3 %), lipids (11.8 %), flavonoids (2.5 %) and phenols (3.9

%). These findings confirm ethanol as an efficient solvent for extracting diverse bioactive compounds from squid biomass (Fig. 3) [25,26].

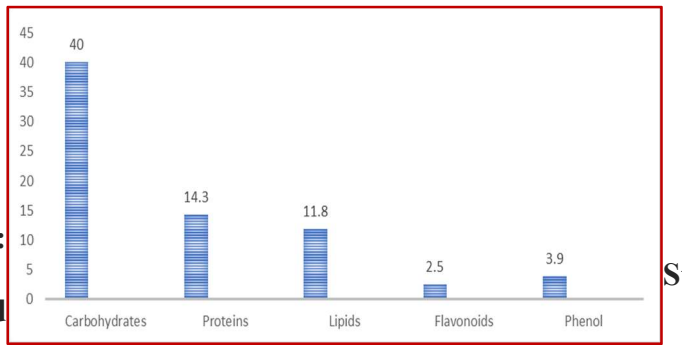

Fig. -4: Spectrophotometric Studies of Marine Squid *Sepioteuthis lessoniana*

GC-MS analysis of marine animals aims to identify and quantify chemical constituents, often to uncover bioactive compounds with pharmaceutical or nutraceutical potential. In this study, the ethanol extract of *Sepioteuthis lessoniana* was analyzed, revealing seven distinct peaks corresponding to seven chemical compounds [27,28]. These included 24 compound like Benzene, 1,2,3-trimethyl- (paint thinners, fuel additives and coating manufacturing), Propane, 1,1,3,3-tetraethoxy (agricultural preservatives), Methyl salicylate (relieve musculoskeletal pain), Benzenepropanoic acid 1-methylethyl ester (synthesis of active ingredients in sunscreen and pharmaceuticals), Tetradecane (pharmaceutical), bis[(2Z)-Hex-2-en-1-yloxy](dimethyl)silane (chemical research uses), Phthalic acid, ethyl isoporpyl ester (anti-inflammatory drug**),** Tetradecanoic acid (as an emulsifier and surfactant**),** Phthalic acid, ethyl oct-3-yl ester (mainly used as a plasticizer), n-Hexadecanoic acid (as a surfactant in soaps, detergents), Heptadecanoic acid (emollients in cosmetics), cis-Vaccenic acid (used as a moisturizer)**,** Ethanol, 2-(octadecyloxy)- (amphiphilic properties), beta-Amyrin (anti-inflammatory, anti-cancer and antioxidant properties), Batilol (cosmetic, pharmaceutical and research industries), Lup-20(29)-en-3-ol, acetate, (3.beta.)-(Anticancer Agent, Pharmaceutical), Dioctyl terephthalate (DOTP) (used as a plasticizer), Cholesta-4,6-dien-3-ol, (3.beta.)-(treat and prevent vitamin D deficiency), Stigmasterol (promote cardiovascular health and reduce inflammation), Cholesterol (pharmaceutical), Cholesta-3,5-dien-7-one (Research & Laboratory Use), Stigmasterol (dietary supplements), Sitosterol (support heart health) and Lupeol (anti-inflammatory, anti-cancer and antioxidant). The results highlight the presence of diverse bioactive molecules in squid, demonstrating its potential as a source of functional compounds for anticancer agent, dietary supplements, anti-inflammatory, anti-cancer and antioxidant properties.

Fig. -5: GC-MS analysis of Ethanol Extract of *Sepioteuthis lessoniana*

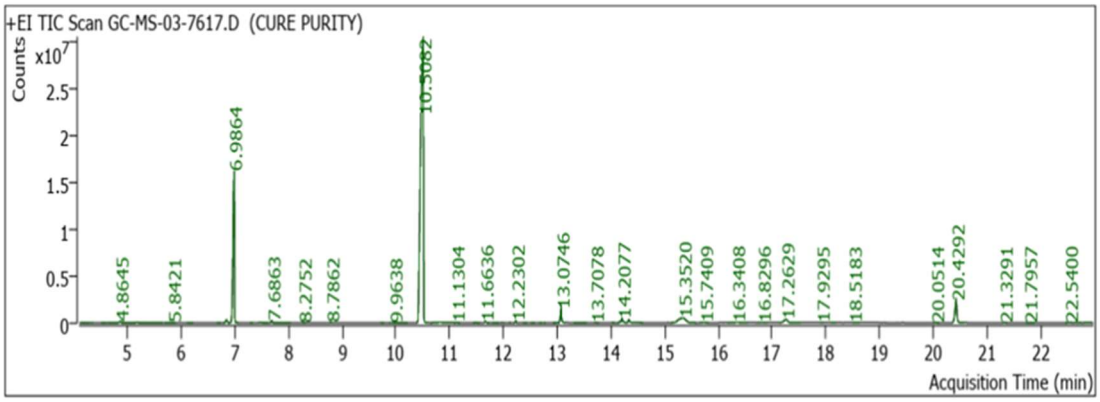

Table -1: GC-MS analysis of Ethanol Extract of *Sepioteuthis lessoniana*

Characterization of Iron Oxide NPs using *Sepioteuthis lessoniana*

The synthesized FeO NPs Sl-FeONPs were characterized using UV–Vis spectroscopy, FTIR, SEM and EDAX to confirm their formation, composition, and morphology. The room-temperature UV–Vis spectrum of FeO-NPs exhibited a prominent absorption peak at 298–301 nm (Fig. 6), which is consistent with the characteristic surface plasmon resonance of FeO NPs, as previously reported [10]. This peak confirms successful nanoparticle formation and aligns well with recent studies on Sl-FeONAs which reported similar absorption maxima within the 290–310 nm range, depending on the reducing agent and particle size. FTIR analysis revealed broad bands at 3350–3450 cm^{-1}, attributed to O–H stretching vibrations from carbohydrates, proteins, and polyphenolic groups capping the nanoparticles. Additional bands at 3700 cm^{-1} and 3100 cm^{-1} correspond to phenolic O–H stretching, while the region 2260–2100 cm^{-1} indicates C=C stretching, suggesting the presence of residual biomolecules from the squid extract. Peaks at 1120–1160 cm^{-1} and 1240–1340 cm^{-1} correspond to C–O–C polysaccharides and C–N amides, respectively. The Fe–O stretching vibrations were observed at 620 and 459 cm^{-1}, confirming the characteristic iron oxide lattice vibrations. These functional groups are consistent with previous green-synthesized Sl-FeONPs. The single phase and crystalline character of iron oxide nanoparticles have been verified by Xray powder diffraction (XRD) spectra. FeONPs development has been verified by Xray diffractive analysis. The crystalline nature of the particles was explained by the XRD spectra. There are different peaks of iron nanoparticles at 31.69 and 75.14 which are Miller indexed to 123 and 372.The distinct analysis of XRD confirms the trigonal rhombohedral morphology of IONPs, which is confirmed through JCPD card No. 96-101-1241[33,34].

S.No	Chemical Compounds	RT	Peak Area	Molecular weight	Molecular formula	Application
1	Benzene, 1,2,3-trimethyl-	4.8645	377684	120.1916	C_9H_{12}	paint thinners, fuel additives, and coating manufacturing
2	Propane, 1,1,3,3-tetraethoxy-	5.8421	46643	220.3059	$C_{11}H_{24}O_4$	used in the production of agricultural preservatives.
3	Methyl salicylate	6.9864	31030155	152.1473	$C_8H_8O_3$	acts as a flavoring agent in toothpaste and candies, and as a fragrance in cosmetics
4	Benzenepropanoic acid 1-methylethyl ester	8.2752	11296	192.2542	$C_{12}H_{16}O_2$	synthesis of active ingredients in sunscreen and pharmaceuticals
5	Tetradecane	8.7862	104132	198.3880	$C_{14}H_{30}$	pharmaceutical, and laboratory applications
6	bis[(2Z)-Hex-2-en-1-yloxy](dimethyl)silane	9.9638	75246	256.46	$C_{14}H_{28}O_2Si$	its main uses are in chemical research
7	Phthalic acid, ethyl isoporpyl ester	11.1304	137856	236.26	$C_{13}H_{16}O_4$	It acts as a primary metabolite of ibuprofen in humans
8	Tetradecanoic acid	11.6636	295337	228.3709	$C_{14}H_{28}O_2$	as an emulsifier, personal care products like soaps, shampoos, and shaving creams.
9	Phthalic acid, ethyl oct-3-yl ester	12.2302	240520	306.4	$C_{18}H_{26}O_4$	mainly used as a plasticizer
10	n-Hexadecanoic acid	13.0746	2536051	256.4241	$C_{16}H_{32}O_2$	as a surfactant in soaps, detergents, and cosmetics (as an emollient)
11	Heptadecanoic acid	13.7078	62829	270.4507	$C_{17}H_{34}O_2$	emollients in cosmetics, skin penetration enhancers in topicals, and as industrial solvents or flavoring agents
12	cis-Vaccenic acid	14.2077	1218967	282.4614	$C_{18}H_{34}O_2$	used as a moisturizer and emulsifier in cosmetics, a cleaning agent in soaps, and an industrial lubricant.
13	Lupeol	15.3520	4854469	426.7174	$C_{30}H_{50}O$	anti-inflammatory, anti-cancer, and antioxidant properties
14	Ethanol, 2-(octadecyloxy)-	15.7409	129775	314.5463	$C_{20}H_{42}O_2$	amphiphilic properties, acting as an emulsifier, solubilizer, and stabilizer in various industries
15	beta.-Amyrin	16.3408	430098	426.7174	$C_{30}H_{50}O$	anti-inflammatory, anti-cancer, and antioxidant properties
16	Batilol	16.8296	53425	344.5723	$C_{21}H_{44}O_3$	used in the cosmetic, pharmaceutical, and research industries
17	Lup-20(29)-en-3-ol, acetate, (3.beta.)-	17.2629	1665552	468.7541	$C_{32}H_{52}O_2$	Anticancer Agent,Pharmaceutical Research & Drug Development,Cosmetics and Skincare,Antifungal and Antibacterial.
18	Dioctyl terephthalate (DOTP)	17.9295	10600	490.72	$C_{32}H_{54}O_4$	used as a plasticizer and softening agent
19	Cholesta-4,6-dien-3-ol, (3.beta.)-	18.5183	33073	384.6377	$C_{27}H_{44}O$	treat and prevent vitamin D deficiency, maintain healthy bones/teeth by aiding calcium absorption, and support immune/muscle function.
20	Stigmasterol	20.0514	25906	412.6908	$C_{29}H_{48}O$	lower LDL cholesterol, promote cardiovascular health, and reduce inflammation
21	Cholesterol	20.4292	6178712	386.6535	$C_{27}H_{46}O$	it is used as an emulsifying agent in pharmaceutical and dermal
22	Cholesta-3,5-dien-7-one	21.3291	58360	382.62	$C_{27}H42O$	Research & Laboratory Use &Biochemical Research
23	Stigmasterol	21.7957	33284	412.6908	$C_{29}H_{48}O$	used in functional foods, dietary supplements, and for synthesizing steroid hormones
24	Sitosterol	22.5400	108977	414.7067	$C_{29}H_{50}O$	used in dietary supplements and support heart health.

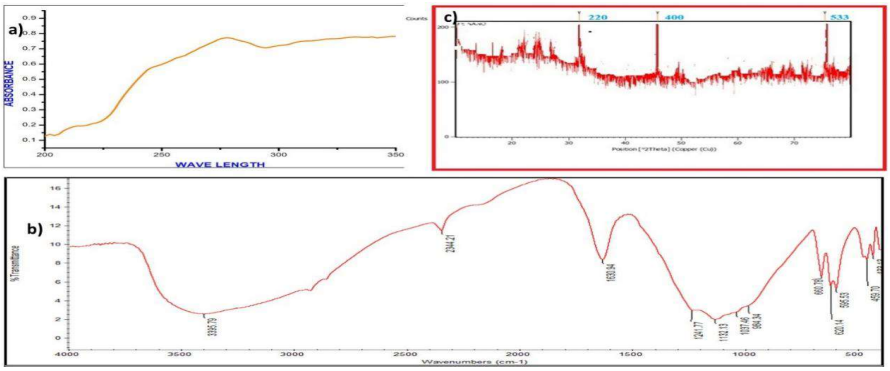

Fig. -5: UV, XRD and FT-IR Spectrum for Marine Squid ethanol extract of *Sepioteuthis lessoniana*

A common method for determining the structure of nanomaterials is the precise SEM examination. This device allows for the study of clear, low- to high magnified pictures down to the nanometer range. The shape of synthesized FeONPs appears to be a spherical in shape. The size of the iron oxide nanoparticles was determined to be between 44 and 81 nm based on the SEM image. The majority of the produced nanoparticles had a spherical appearance, and in a limited number of instances, they formed tiny aggregates. TEM analysis showed polydisperse shape of Sl-FeONPs with diameters ranging from 80 to 180 nanometers.

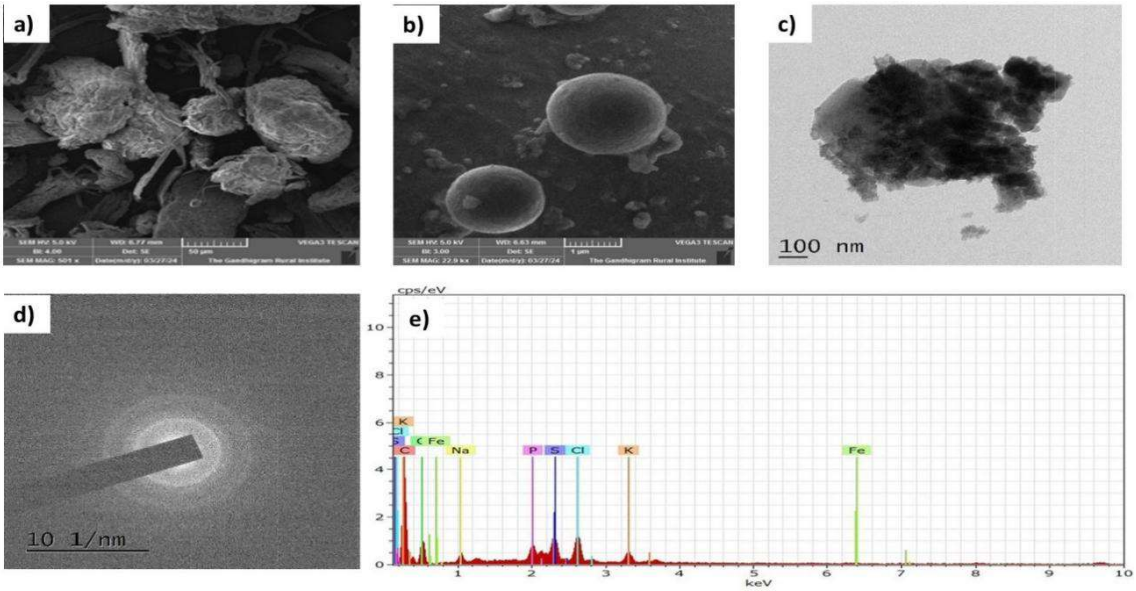

Fig.-6: SEM,EDAX Spectrum for Marine Squid ethanol extract of *Sepioteuthis lessoniana*

Adsorption efficacy of Sl-FeO NPs

Adsorption of a standard calibration curve was constructed using known concentrations of iron oxide nanoparticles (FeO NPs) in the absence of adsorbent. The adsorption performance of FeO nanoparticles synthesized using marine squid extract was systematically evaluated by

varying key operational parameters such as adsorbent dosage, dye concentration, pH, and contact time. The concentration range studied was 40–250 µg in 50 mL solution. The absorbance increased linearly with increasing nanoparticle concentration, confirming adherence to Beer–Lambert's law within the studied range. The linear relationship between absorbance and concentration demonstrated good analytical sensitivity and was used to determine unknown residual concentrations in subsequent adsorption experiments.

Effect of Adsorbent Dosage

The influence of adsorbent dosage (20–120 mg) on IONPs removal was investigated at an initial concentration of 250 µg L^{-1}, pH 6 and contact time of 60 min. The effects of key parameters such as contact time (10–60 min), adsorbent dosage (20–120 mg), dye concentration (40–250 mg/L) and pH (2–12) were systematically examined to determine their influence on dye removal efficiency. The adsorption efficiency increased from 45% to 82 % as the adsorbent dosage increased from 20 to 120 mg. The removal of methylene red (MR) dye improved from approximately 45% at 20 mg to about 82 % at 120 mg. This enhancement is attributed to the increased availability of active adsorption sites and greater surface area at higher dosages, facilitating more dye–adsorbent interactions[35,36] .

Effect of Initial Dye Concentration

The concentration range studied was 40–250 µg in 50 mL solution. The absorbance increased linearly with increasing nanoparticle concentration, confirming adherence to Beer–Lambert's law within the studied range. The linear relationship between absorbance and concentration demonstrated good analytical sensitivity and was used to determine unknown residual concentrations in subsequent adsorption experiments. The adsorption capacity was also influenced by the initial dye concentration (40–250 mg/L). The removal efficiency increased steadily, reaching a maximum of around 92 % at 250 mg/L. At higher concentrations, the driving force for mass transfer increases, enhancing the interaction between dye molecules and FeO NPs surfaces until saturation is approached.

Effect of pH

The pH of the solution played a crucial role in adsorption efficiency. The removal efficiency increased from 30% at pH 2 to a maximum of 88 % at pH 6, after which it declined at higher pH values. This behavior indicates that slightly acidic conditions favor adsorption, likely due to optimal surface charge conditions that enhance electrostatic attraction between the dye molecules and nanoparticle surface. At alkaline pH, competition with hydroxyl ions reduces adsorption efficiency.

Effect of Contact Time

Contact time studies revealed a rapid increase in adsorption efficiency within the first 30 minutes, followed by a gradual approach to equilibrium at 60 minutes. The removal efficiency increased from 45% at 10 min to 88 % at 60 min. The initial rapid phase is due to abundant vacant active sites, while the later slower phase corresponds to site saturation and equilibrium attainment.Under optimized conditions (adsorbent dosage: 120 mg, dye concentration: 250 mg/L, pH: 6, contact time: 60 min), the FeO NPs synthesized using marine squid extract exhibited high adsorption efficiency (90 %), demonstrating their potential as an effective, eco-friendly adsorbent for dye removal from aqueous systems.

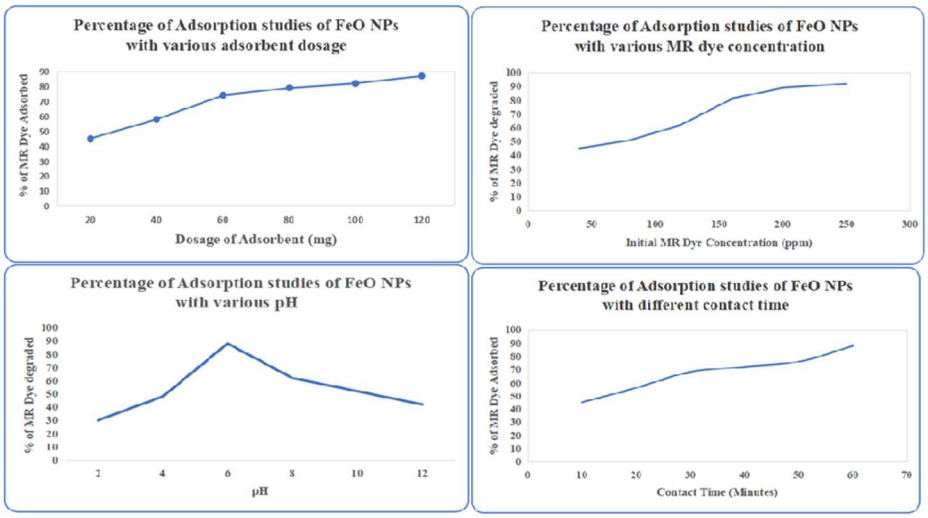

Fig. -7: Adsorption efficacy of Sl-FeO NPs Marine Squid ethanol extract of *Sepioteuthis lessoniana*

UV-Vis Interpretation for Adsorption Studies of Sl-FeO NPs

The UV–Vis spectrum of Sl-FeO shows a broad absorption band in the region of ~250–320 nm, with a gradual increase in absorbance toward higher wavelengths. This characteristic absorption confirms the formation of iron oxide nanoparticles. Additionally, the biomolecules present in squid extract (proteins, amino acids, and polysaccharides) act as reducing and stabilizing agents, contributing to the smooth absorption profile without sharp peaks. The UV–Vis spectrum of methyl red (MR) dye exhibits a peak at 218 nm corresponding to $\pi \rightarrow \pi^*$ transitions of the aromatic ring. A prominent peak at 520 nm, attributed to $n \rightarrow \pi^*$ transitions associated with the azo (-N=N-) chromophore. The strong visible region absorption confirms the intense color of methyl red and its suitability as a model organic pollutant in adsorption studies. After treatment with Sl-FeO NPs, the UV–Vis spectrum of methyl red dye shows a significant decrease in absorbance intensity, particularly at the characteristic peak around 518 nm. Sl-FeO NPs exhibit excellent adsorption efficiency for methyl red dye removal, supporting their application in eco-friendly wastewater treatment[31-34].

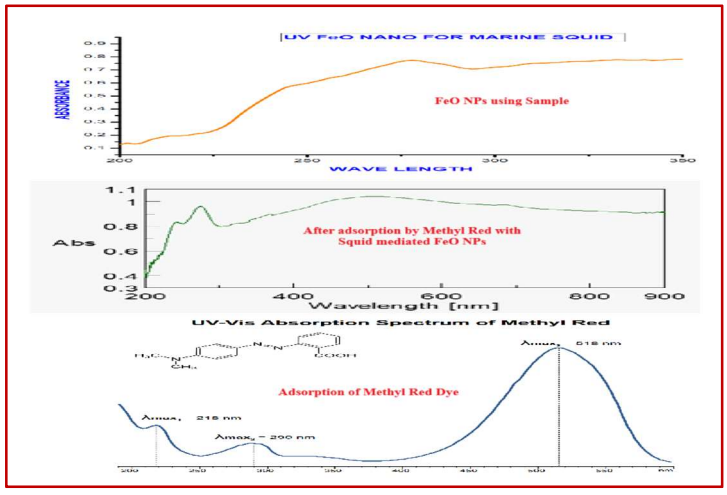

Fig. -8: UV-Vis Interpretation for Adsorption Studies of Sl-FeO NPs

FT-IR Interpretation for Adsorption Studies

The broad absorption band observed around 3400–3450 cm^{-1} in spectra A and C corresponds to the stretching vibration of –OH groups and adsorbed water molecules present in the marine squid extract capped IONPs. After adsorption of methyl red dye, this peak becomes broader and slightly shifted, indicating hydrogen bonding interactions between hydroxyl groups of the nanoparticle surface and dye molecules. The absorption peak near 2920–2850 cm^{-1} is attributed to C–H stretching vibrations of aliphatic compounds originating from bioactive constituents of the marine squid extract. A reduction in intensity after adsorption suggests surface interaction with methyl red molecules.

In spectrum B (methyl red dye), characteristic peaks observed around 1600–1500 cm^{-1} correspond to the azo (–N=N–) stretching vibration and aromatic C=C stretching of methyl red. After adsorption (spectrum C), these peaks shift slightly and decrease in intensity, confirming the attachment of dye molecules onto the IONPs surface. The prominent band observed around 1400–1450 cm^{-1} is assigned to C–N stretching and aromatic ring vibrations of methyl red dye. The shift in this peak after adsorption indicates electrostatic interaction between the negatively charged dye molecules and positively active adsorption sites on IONPs [39,40].

The peaks appearing in the region of 1100–1000 cm^{-1} are related to C–O and C–O–C stretching vibrations of biomolecules present in the squid extract acting as stabilizing agents. Changes in this region after adsorption suggest participation of oxygen-containing functional groups in dye binding. The characteristic absorption band below 600 cm^{-1}, particularly around 520–580 cm^{-1}, confirms the presence of Fe–O stretching vibrations, indicating the formation of IONPs. The slight shift of this peak after adsorption demonstrates the interaction of methyl red dye with the IONPs surface [41]. the FTIR results confirm that functional groups such as hydroxyl, amino, carbonyl, and Fe–O groups present on marine squid extract-mediated FeO nanoparticles actively participate in the adsorption of methyl red dye through hydrogen bonding, electrostatic attraction, and surface complexation mechanisms.

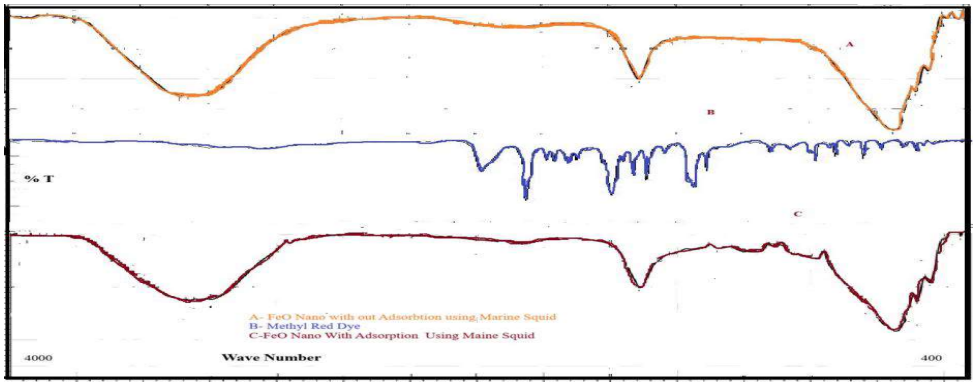

Fig. -9: FT-IR Interpretation for Adsorption Studies of Sl-FeO NPs

The adsorption isotherm

The adsorption isotherm for the removal of methyl red (MR) dye by bio synthesized IO NPs were analyzed using the Langmuir, Freundlich and Temkin models to understand the interaction between the adsorbate and adsorbent surfaces (Fig. - 12 a–c). The Langmuir

isotherm indicated a maximum monolayer adsorption capacity (Qe) of 42.34 mg/g, with an adsorption intensity factor (RL < 1) confirming the favourability of the process and a correlation coefficient (R^2) of 0.6593. The Freundlich isotherm also showed a strong correlation (R^2 = 0.6624), with a Freundlich constant (KF) of 22.45 (mg/g)(mg/L)^n and an exponent (1/n = 0.3928), suggesting a heterogeneous surface and multilayer adsorption. The lower Reduced Chi-Square value obtained for the Freundlich model compared to the Langmuir model indicates a better fit, implying that the adsorption process is likely heterogeneous in nature. The Temkin isotherm was also evaluated, where the constants BT (J/mol) and AT (L/mg) were determined from the slope and intercept of the plot of Qe versus ln Ce providing information on the binding energy and heat of adsorption. Overall, the Freundlich model best described the adsorption behavior of MR dye onto IONPs, suggesting multilayer adsorption on a heterogeneous surface facilitated by the bioactive compounds from the squid extract. Among the three models, the Langmuir isotherm showed the best fit, indicating monolayer adsorption of contaminants onto IONPs synthesized using *Sepioteuthis lessoniana*. However, the Freundlich model also suggested surface heterogeneity due to bio-organic capping agents, while the Temkin model confirmed adsorbate–adsorbent interactions [38-48].

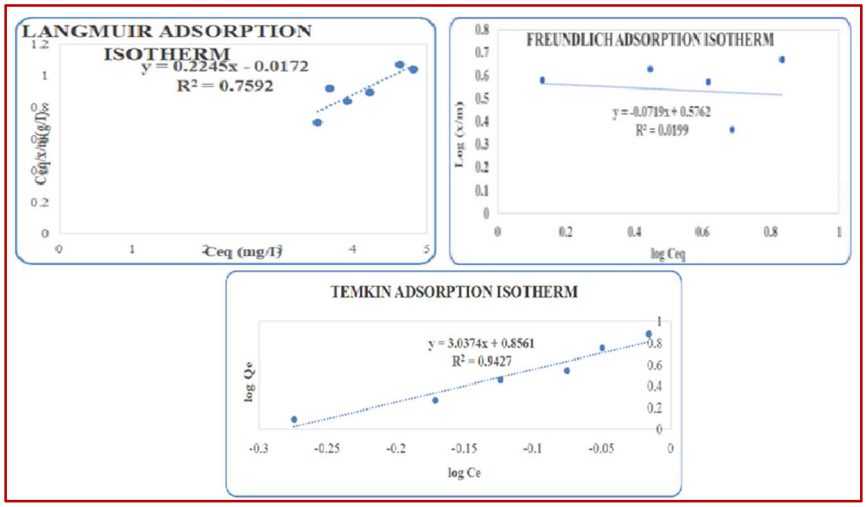

Fig. -10: Langmuir and Frendulich isotherm model for MR dye adsorption onto IONPs using marine squid extract at pH 6, a contact time of 60 min, an adsorbent dosage of 120 mg/50 mL and a temperature of 30 ◦C

Mosquito Larvicidal Assay of Sl-FeO NPs

The WHO standard [49] was followed with modifications as outlined by Suresh *et al.,*[50] in order to assess the toxicity of FeO NPs made using *U. chamae*. An 80 well tissue culture plate was used, and 10 second instar larvae of *A. gambae* and *C. quinquefasciatus* were placed in each well, which contained 3 mL of the test medium. Iron nanoparticles in varying concentrations were added to distilled water to create the test medium. The World Health Organization (WHO) larval bioassay method provides a standardized and detailed protocol for evaluating the toxic effects of insecticides and bioactive compounds against mosquito larvae. In this method, a defined number of mosquito larvae are introduced into a measured volume of water containing different concentrations of the test substance and larval mortality is recorded after

a specified exposure period. This assay is widely used to determine the larvicidal efficacy of synthetic and squid-mediated IONPs against mosquito vectors [51].

Second instar mosquito larvae were exposed to different concentrations of synthesized IONPs under controlled laboratory conditions to evaluate their larvicidal activity. A fixed number of larvae were introduced into test solutions containing varying nanoparticle concentrations and mortality was recorded after the required exposure period. The percentage of larval mortality increased with increasing nanoparticle concentration, indicating a concentration-dependent toxic effect. These observations confirm that nanoparticles possess effective larvicidal potential against mosquito larvae and can be utilized for mosquito vector control applications [52].

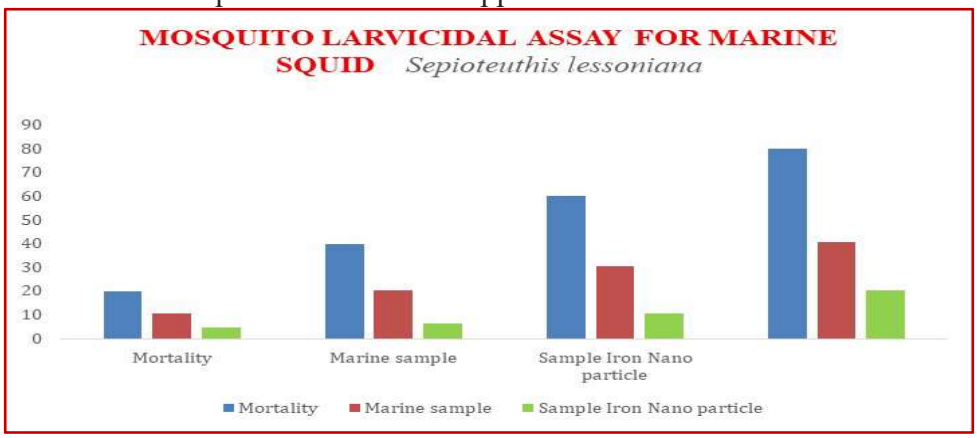

Fig. -11: Mosquito Larvicidal Assay of Sl-FeO NPs

HEMOLYSIS ASSAY

The addition of FeO NPs using ethanol extract of marine squid *Sepioteuthis lessoniana* to blood will result in hemolysis due to erythrocyte clumping and crystal-induced damage [37]. 28 However, up to 5 µg/mL of CaO NPs displayed 0.591 hemolysis ratio, indicating nonhemolytic. When a larger quantity of CaO NPs NPs, 10, 25, 50 and 100 µg/mL mixed with blood and hemolytic activity increased to 0.617, 0.683, 0.715 and 0.773, respectively. This shows that NPs with a greater concentration of CaO NPs may display a minor hemolytic effect. CaO NPs and RBC interaction could have led to the oxidative stress thereby increasing concentration of hemolytic activity . In addition, In the future, the hemolytic impact of large concentrations of CaO NPs NPs can be mitigated by optimizing their surface charge [38].

Direct contact between IONPs and red blood cells (RBCs) can disrupt membrane integrity, resulting in hemolysis. Nanoparticles may interact with the phospholipid bilayer of RBC membranes, causing structural alterations, membrane permeability changes and eventual rupture of the cells. In addition, the generation of oxidative stress (OS) by nanoparticles is considered one of the major mechanisms responsible for RBC damage. Therefore, hemolytic studies are essential to evaluate the biocompatibility and biosafety of IONPs for biomedical applications [53].

The percentage of hemolysis increased significantly with increasing concentrations of IONPs, indicating a clear concentration-dependent hemolytic activity. At lower IONPs concentrations, minimal damage to red blood cells (RBCs) was observed whereas higher concentrations caused greater disruption of the RBC membrane, resulting in increased hemoglobin release. This concentration-dependent behavior suggests that elevated IONPs exposure enhances oxidative stress and membrane interaction leading to higher levels of cell lysis. The results emphasize the importance of optimizing IONPs concentration to ensure biocompatibility and minimize toxic effects in biomedical applications [54].

Table -2: Hemolytic Assay of FeO NPs Using *Sepioteuthis lessoniana*

Sl. No	Concentration of CaO NPs using *Sepioteuthis lessoniana* (µg /ml)	Hemolysis ratio
1	5	0.562
2	10	0.631
3	25	0.694
4	50	0.738
5	100	0.781

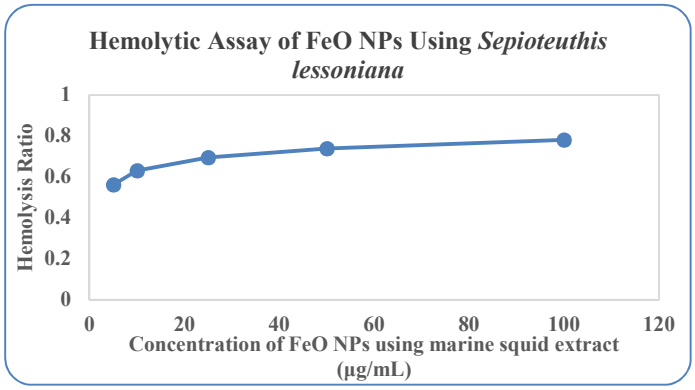

Fig. -12: Hemolytic Assay of FeO NPs Using *Sepioteuthis lessoniana*

CONCLUSION

This study reports an eco-friendly approach for synthesizing iron oxide nanoparticles using marine squid (*Sepioteuthis lessoniana*) biomass as a natural reducing and stabilizing agent. The biosynthesized nanoparticles (Sl-FeONAs) were evaluated for adsorptive removal of methyl red (MR) dye, larvicidal activity, and hemolytic safety. Structural and morphological characteristics of Sl-FeONAs were confirmed by UV–visible spectroscopy, FTIR, XRD, SEM and EDX analyses, indicating the successful formation of nanoscale iron oxide particles capped with biomolecules. Adsorption experiments demonstrated rapid dye removal, with maximum efficiency of approximately **88%** under optimal conditions (pH 6, 60 min contact time, and suitable adsorbent dosage). The adsorption behavior was better described by the **Freundlich isotherm model**, suggesting heterogeneous surface adsorption and multilayer formation. In addition, the synthesized nanoparticles exhibited significant larvicidal activity against mosquito larvae while showing minimal hemolytic effects at lower concentrations, indicating good biocompatibility. These findings highlight the potential of marine biomass-mediated iron oxide nanoparticles as sustainable multifunctional materials for wastewater treatment and vector control applications.

ACKNOWLEDGMENTS

Sincere thanks to the management of A.P.C. Mahalaxmi College for Women, Thoothukudi, India for providing the facilities and support to carry out work.

CONFLICT OF INTERESTS

The authors declare that there is no conflict of interest.

AUTHOR CONTRIBUTIONS

The poresent work is related to *SDG-14; Life Below Water*, Allthe authors contributed significantly to this manuscript, participated in reviewing/editing and approved the final draft for publication. The research profile of the authors can be verified from their ORCID ids, given below.

A. Malarvizhi https://orcid.org/0009-0009-7304-4390
C. Stella Packiam https://orcid.org/0000-0002-7764-9444
M. I. Delighta Mano Joyce https://orcid.org/0009-0000-0729-0395
A. Dhivya https://orcid.org/0000-0002-8379-1711

REFERENCES

References in the text should be cited as super-scripted and at the end of the sentence. Please rectify this mistake also, if there. Listing of References must be strictly as per the STYLE of the journal **(Please refer Journal's Guidelines and any published paper from the current issue)**. **Use Complete names of the Journals in reference (not abbreviations), Also, Mention DOI with references, wherever possible,** which may otherwise cause unnecessary delay in publication of your paper. You are requested to re-check all your references with respect to its Volume No., Page No., Full Name of Journal / Name of Publisher, Year etc. and format according to the Guidelines of the Journal.

REFERENCES

1. N. D. Lai, D. T. C. Nguyen, *J Ind Eng Chem,* **157**, 57-61(2025), **DOI:10.1016/j.jiec.2025.10.041**

2. Y. N. Teixeira, J. M. Menezes, R. N. P. Teixeira, F. J. Paula Filho and T. M. Oliveira, *Textiles*, **3(1),** 52-65(2023), **DOI:10.3390/textiles3010005**.

3. I. Khan, K. Saeed, I. Khan, *Arab J Chem*, **16(4)**, 104756(2023), **DOI:10.1016/j.arabjc.2023.104756**.S

4. A. Sharma, V. K. Gupta, D. Pathania and N. C. Kothiyal, *Nanomaterials*, **13(3)**, 564(2023), **DOI:10.3390/nano13030564**.

5. P. Priya, N. A. Naveen, K. K. Kaur and A. K. Sidhu, *Front Nanotechnol*, 2021, 3, 655062(2021), Published June 15, 2021. **DOI:10.3389/fnano.2021.655062.**

6. S. Ali, A. Zahid and S. T. Shahid, In: *IntechOpen*, Published June 24, 2023. DOI:10.5772/intechopen.1001910.

7. J. Narware, S. P. Singh, N. Manzar and A. S. Kashyap, *Front Microbiol*, **14**, 1159251(2023), Published 2023 Apr 17. **DOI:10.3389/fmicb.2023.1159251**.

8. V. Jadhav, A. Bhagare, and R. Gurgude, *Nanoscale Res Lett*, 20(1), 125(2025), Published 2025 Jul 31, **DOI:10.1186/s11671-025-04322-**7.

9. World Health Organization, *Guidelines for laboratory and field testing of mosquito larvicides,* WHO Press, 10-11(2005).

10. G. Benelli, R. Pavela and A. Canale, *Acta Trop*, **210**, 105504(2020), **DOI:10.1016/j.actatropica.2020.105504.**

11. E. D. de Ávila, B. van Oirschot and J. van den Beucken, *Nanomaterials*, **12(8)**, 1311, (2022), **DOI:10.3390/nano12081311**.

12. F. W. Fales, J. A. Russell and J. N. Fain, *Clin Chem*, **7(4),** 289-303(1961), **DOI:10.1093/clinchem/7.4.289.**

13. E. Van Handel, *J Biochem Biophys Methods*, **4(3-4)**, 227-231(1981), **DOI:10.1016/0165-022X(81)90060-9**

14. B. R. Hewitt, *Nature*, **182**, 246-247(1958), **DOI:10.1038/182246b0**

15. J. H. Waterborg and H. R. Matthews, *Methods Mol Biol*, **1**, 1-3(1984), **DOI:10.1385/0-89603-062-8:1**

16. J. H. BRAGDON, *The Journal of Biological Chemistry,* **190**, no. 2 , 513-517(1951),

17.J. D. Everette, Q. M. Bryant, A. M. Green, Y. A. Abbey, G. W. Wangila and R. B. Walker, *J Agric Food Chem*, **58(14)**, 8139-8144(2010), **DOI:10.1021/jf1005935**

18. E. J. Lee, N. Nomura, B. S. Patil and K. S. Yoo, *Int J Food Sci Technol*, **49(11)**, 2364-2372(2014), **DOI:10.1111/ijfs.12557**

19. M. M. Rahman, M. M. Islam and M. S. Hossain, *J Appl Phycol*, (2026), **DOI:10.1007/s10811-026-03846-4**

20. D. Ferreira, J. Silva and L. Pereira, *Mar Drugs*, **23(2)**, 114(2025), **DOI:10.3390/md23020114**.

21. E. M. Silva, J. N. S. Souza, H. Rogez, J. F. Rees and Y. Larondelle , *Food Chem*, **101(3)**, 1012-1018(2020), **DOI:10.1016/S0308-8146(20)31842-1.**

22. J. B. Harborne, S. D. Sarker and L. Nahar, *Natural Products Isolation*. *Methods in Molecular Biology,* **Vol 1880**. Humana Press, 115-132(2019), **DOI:10.1007/978-1-4939-8778-8_12.**

23. G. Elango, S. M. Roopan, N. A. Al-Dhabi, M. V. Arasu, and K. I. Damodharan, *Mater Today Proc*, **45**, 2231-2235(2021), **DOI:10.1016/j.matpr.2020.11.814.**

24. J. Singh, T. Dutta, K. H. Kim, M. Rawat, P. Samddar and P. Kumar, *Nanomaterials*, **12(18)**, 3254(2022), **DOI:10.3390/nano12183254.**

25. S. P. Aubourg, M. Trigo, M. J. González, S. Lois and I. Medina, *Foods*, **11(15)**, 2188(2022), **DOI:10.3390/foods11152188**.

26. S. P. Aubourg, A. Rodríguez, M. Trigo and I. Medina, *Foods*, **12(14)**, 2649(2023), **DOI:10.3390/foods12142649**.

27. V. D. Rajeswari, S. Ramachandran, and N. M. Prabhu, *Heliyon*, **6(12)**, e05743(2020), **DOI:10.1016/j.heliyon.2020.e05743**.

28. S. K. Kim, Y. D. Ravichandran, S. B. Khan and Y. T. Kim, *Mar Drugs*, **19(8)**, 441(2021), **DOI:10.3390/md19080441**.

29. G. S. Kiran, A P. Lipton , S. Priyadharshini S, *Journal of Applied Microbiology*, **125(3)**, 723-734(2018), **DOI:10.1111/jam.13965.**

30. G. Benelli, *Asian Pacific Journal of Tropical Biomedicine*, **6(4)**, 353-356(2016), **DOI: 10.1016/j.apjtb.2015.10.015.**

31. M. Govindarajan, N. S. Alharbi, S. Kadaikunnan, J. M. Khaled and G. Benelli, *Mater Today Proc*, **45**, 2236-2241(2021), **DOI:10.1016/j.matpr.2020.12.215.**

32. Benelli G, Pavela R, Canale A, et al. Green-synthesized nanoparticles in mosquito control: current knowledge and future challenges. *Acta Trop*, **210**, 105504(2020), **DOI:10.1016/j.actatropica.2020.105504.**

33. J. Singh, T. Dutta, K. H. Kim, M. Rawat, P. Samddar and P. Kumar, *Nanomaterials*, **12(18)**, 3254(2022), **DOI:10.3390/nano12183254**.

34. G. Elango, S. M. Roopan, N. A. Al-Dhabi, M. V. Arasu and K. I. Damodharan, *Mater Today Proc*, **45**, 2231-2235(2021), **DOI:10.1016/j.matpr.2020.11.814.**

35. M. J. Ahmed and S. K. Theydan, *Chem Eng J*, **420**, 129700(2021), **DOI:10.1016/j.cej.2021.129700.**

36. D. Pathania, S. Sharma and P. Singh, *Water* , **14(9)**, 1372(2022), **DOI:10.3390/w14091372.**

37. E. D. de Ávila, B. van Oirschot and J. van den Beucken, . *Nanomaterials,* 12(8), 1311(2022), **DOI:10.3390/nano12081311**.

38. B. Fadeel, L. Farcal and B. Hardy, *Nat Nanotechnol*, 16(1), 1-12(2021), **DOI:10.1038/s41565-020-00815-6.**
39. S. Khandelwal, N.R. Devi, M. Subramaniyan and S. Pappu, *3 Biotech*, **13(12)**, 418(2023), **DOI:10.1007/s13205-023-03809-8**
40**.** R. Shivani, R.S. Bhat, S.P. Sajankila and A.G. Bindu, *Journal: Applied Physics A,* **131(8)**, 649(2025), **DOI: 10.1007/s00339-025-08775-6.**
41. M. R. Delgado, *Appl Sci*. **10(23)**, 8589(2020), **DOI:10.3390/app10238589B**.
42. V.T. Hau, N.T. Chinh, P.H. Linh, N.T. T. Loan, N. T. M. Viet, D. D. Dung and N. Q. Dung, *RSC advances*, **15(59)**, 50795-50809(2025), **DOI:10.1039/D5RA07081C.**
43. H. K. Hami, *Appl Water Sci.* **15**, 2682(2025), **DOI:10.1007/s13201-025-02682-0.**
44. I. Langmuir, *Journal of the American Chemical society*, ***40*(9),** 1361-1403 (1918), **DOI: https://doi.org/10.1021/ja02242a004**.
45. D. Chattoraj and H.M. Freundlich, *Journal of Physical Chemistry A*, **57**, 385-470 (1906), **DOI:10.1515/zpch-1907-5723** .
46. K. Y. Foo, and B.H. Hameed*, Chemical Engineering Journal,* **156**, 2, 10(2010), **DOI: https://doi.org/10.1016/j.cej.2009.09.013**.
47. H. N. Tran, S. J. You, A. Hosseini-Bandegharaei, H. P. Chao, *J Environ Chem Eng,* , 5(5), 4268-4280(2017), **DOI:10.1016/j.jece.2017.08.026.**
48. S. Bamford, *PLoS Negl Trop Dis* , **15(1)**, e0008639(2021), **DOI:10.1371/journal.pntd.0008639.**
49. S. Yedgar, G. Barshtein and A. Gural, *Micromachines (Basel),* **13(12)**, 2091(2022), **DOI: 10.3390/mi13122091.**
50. S. Yadav, S. Bhagat, S. Singh and P.K. Maurya, *The Journals of Gerontology, Series A: Biological Sciences and Medical Sciences,* ***79*(11),** glae197, (2024), **DOI: https://doi.org/10.1093/gerona/glae197.**
51.V. A. Ingham, S. Wagstaff, and H. Ranson, *PLoS Negl Trop Dis*, **14(10)**, e0008639(2020), **DOI:10.1371/journal.pntd.0008639**
52 .U.M Gunathilaka, W. de Silva, S. P. Dunuweera and R. Rajapakse, *RSC Adv*. , **11(15)**, 8857-8866(2021) **DOI:10.1039/D1RA00014D**
53. G. M. DeLoid, J. M. Cohen, G. Pyrgiotakis and P. Demokritou, *Nanomaterials (Basel)*, **12(10)**, 1619(2022), **DOI:10.3390/nano12101619.**
54. P. Kesharwani, S. Banerjee and U.Gupta, *Biomaterials*, **276**, 121028(2021), **DOI:10.1016/j.biomaterials.2021.121028**